Available online at www.sciencedirect.com
SCIENCE DIRECT
Journal of Catalysis 229 (2005) 154–162
JOURNAL OF CATALYSIS
www.elsevier.com/locate/jcat

The effect of different types of additives on the catalytic activity of Au/Al_2O_3 in propene total oxidation: transition metal oxides and ceria

Andreea Catalina Gluhoi [a], Nina Bogdanchikova [b], Bernard E. Nieuwenhuys [a,*]

[a] *Department of Heterogeneous Catalysis and Surface Chemistry, Leiden Institute of Chemistry, Leiden University, PO Box 9502, 2300 RA Leiden, The Netherlands*

[b] *Centro de Ciencias de la Materia Condensada-UNAM, Km. 107, Carretera Tijuana-Ensenada, 22800, Ensenada, Baja California, Mexico*

Received 13 August 2004; revised 1 October 2004; accepted 4 October 2004

Available online 8 December 2004

Abstract

The total oxidation of C_3H_6 was investigated over Au/Al_2O_3, and multicomponent $Au/MO_x/Al_2O_3$ (M: Ce, Mn, Co, Fe) catalysts prepared by deposition-precipitation with urea. The catalysts have been characterized by means of X-ray diffraction (XRD), high-resolution transmission electron microscopy (HRTEM), scanning electron microscopy (SEM), total surface area (BET), and diffuse reflectance ultraviolet–visible spectroscopy DR/UV–Vis. Based on this characterization, it was concluded that gold is present as Au^0. The most active catalyst is $Au/CeO_x/Al_2O_3$. Ceria and the transition metal oxides act as cocatalysts. It can supply oxygen via a Mars and van Krevelen mechanism.

Keywords: Gold; Additives; Promoters; Cocatalyst; Ceria; Transition metal oxides; Propene oxidation; Mars and van Krevelen mechanism

1. Introduction

An important class of air pollutants consists of volatile organic compounds (VOCs) from industrial plants and transportation vehicles. Among the potential technologies for VOC abatement, catalytic oxidation is preferred. The intended oxidation products are CO_2 and H_2O, which are eventually accompanied by HCl if the VOCs are chlorinated. Conventionally, catalysts based on noble metals (Pt and Pd) supported on Al_2O_3 or SiO_2 are successfully used to eliminate VOCs by total combustion [1]. However, attention has also been paid to base metals. Cobalt oxide, chromium oxide, and copper oxide are reported to be among the most active oxides in catalytic combustion [2–4]. Furthermore, spinel-like materials ($CoCr_2O_4$, $CuCr_2O_4$, $ZnCr_2O_4$ [5,6]) or perovskite-like compounds ($LaMO_3$ [7,8]) are reported to be promising because of their high activity and stability at high temperatures. The mechanism of the total combustion of VOCs (propane, propene, acrolein, propan-2-ol, and acetone) over Co_3O_4, $MgCr_2O_4$, and CuO was established to be of the Mars and van Krevelen type and proceeds through nucleophilic attack of the lattice oxygen of the above-mentioned oxides [9,10].

Gold, despite its chemical inertness, if present in a massive form, proved to be very active in CO oxidation at very low temperatures when it is highly dispersed and deposited on reducible metal oxides, hydroxides of alkaline earth metals, or amorphous ZrO_2 [11–13]. In addition, it has been demonstrated that gold-based catalysts are catalytically active in other reactions: NO_x reduction [14–16], hydrogenation of unsaturated hydrocarbons [17], WGS reaction [18], NH_3 oxidation [19], and total oxidation of VOCs (i.e., 2-propanol, methanol, and toluene) [20,21]. For the latter, the catalytic activity of Au/Al_2O_3 and Au/CeO_2 has been explained on the basis of the capacity of gold to increase the mobility of the metal oxide lattice oxygen, which is involved in the VOCs oxidation through a Mars and van Krevelen mechanism [20,21].

However, there are still disputes regarding the active form of Au: is it zerovalent or oxidized [22], or is the simulta-

* Corresponding author.
E-mail address: b.nieuwe@chem.leidenuniv.nl (B.E. Nieuwenhuys).

0021-9517/$ – see front matter
doi:10.1016/j.jcat.2004.10.003

neous presence of metallic gold atoms adjacent to cationic gold required [23–25]? Furthermore, the role of water is unclear, inasmuch as both beneficial [26,27] and detrimental effects [28,29] of water on the catalytic activity of gold have been reported. In addition, the role of additives is still under discussion. There is a general consensus that certain additives/supports prevent small gold crystallites from sintering under mild reaction conditions. It has also been proposed that the interface gold-metal oxide may play an important role in the activation of oxygen [30,31].

The aim of this paper is to elucidate for the present case study:

(a) The nature of the gold (metallic or ionic?) in the gold-based catalysts used;
(b) The role of the additive: is it a chemical promoter, a structural promoter, or a cocatalyst?

A chemical promoter implies that the additive, though not active itself, improves the effectiveness of the catalyst by chemical means. A structural promoter increases the catalytic activity by modifying the structure of the catalyst, and a cocatalyst has an active role in the catalytic action and acts along with the main catalyst.

More specifically, we report here on the catalytic oxidation of propene as one hydrocarbon representative of automotive emission [32], over Au supported on alumina, with ceria, Co_3O_4, MnO_2, and Fe_2O_3 used as additives.

All of the above-mentioned multicomponent catalysts have been characterized by means of different techniques, such as atomic absorption spectroscopy (AAS), XRD, BET, HRTEM, SEM, and DR/UV–Vis, and attempts have been made to correlate the catalytic activity with the structure/composition of the catalysts.

2. Experimental

2.1. Catalyst preparation

Mixed oxides, MO_x/Al_2O_3, were prepared by vacuum impregnation of γ-Al_2O_3 (Engelhard Al-4172P, $S_{BET} = 275\ m^2\ g^{-1}$, pore volume: $3\ ml\ g^{-1}$) with the corresponding nitrates of Ce, Co, Mn, and Fe (Aldrich products; > 99.9% purity). After drying for at least 16 h at 80 °C in static air, the mixed oxides were subjected to calcination in O_2 flow at 350 °C for 2 h. The prepared mixed oxides typically have an M:Al atomic ratio of 1:15.

Gold was added to Al_2O_3 or MO_x/Al_2O_3 via homogeneous deposition-precipitation (HDP), with the use of urea as a precipitating agent and $HAuCl_4 \cdot 3H_2O$ (Aldrich; 99.99%) as the gold precursor. Details of the preparation procedure have been reported elsewhere [16]. The solution pH at which the deposition of $HAuCl_4$ takes place on the support is of crucial importance to achieving the most active form of Au and depends, besides other factors, on the so-called "point of zero charge" (PZC) of the support that is used. Details concerning the PZC of various oxides may be found elsewhere [33]. For the present case, the final pH solution was 8.5. The filtered powders were thoroughly washed to remove Cl^- residues. All catalysts were calcined in O_2 flow at 300 °C for 2 h. The intended gold loading was 5 wt%.

2.2. Catalyst characterization

The gold loading was measured by atomic absorption spectroscopy (AAS) with a Perkin-Elmer 3100 spectrometer with an air/acetylene flame [16]. For that purpose, the catalyst was dissolved in aqua regia ($3HCl:HNO_3$), and the solution was diluted with demineralized water before the analysis was performed.

BET surface areas of the catalysts were measured by N_2 physisorption at −196 °C with an automatic Qsurf M1 analyzer (Thermo Finnigan). Before each measurement the catalyst was degassed for 2 h in helium at 200 °C to remove the adsorbed impurities. For each measurement at least three points were taken in account to calculate the total surface area of the samples.

XRD measurements were carried out on a Philips Goniometer PW 1050/25 diffractometer equipped with a PW Cu 2103/00 X-ray tube operating at 50 kV and 40 mA. The average gold particle size was estimated from XRD line broadening with the Scherrer equation.

DR/UV–Vis spectroscopy experiments were performed with two commercial units: a Perkin-Elmer Spectrometer, Lambda 900, and a CARY 300 SCAN (Varian). The measurements were performed on air-exposed samples between 200 and 850 nm.

HRTEM measurements were made with a JEOL 2010 microscope with a point-to-point resolution better than 0.19 nm.

SEM and energy dispersive spectroscopy (EDS) data were obtained with a JEOL (JSM 5300) microscope.

2.3. Catalytic activity measurements

Propene (C_3H_6) oxidation was carried out in a lab-scale fixed-bed reactor in which typically 0.2 g of catalyst was loaded. Prior to each measurement, the catalyst was reduced in situ at 300 °C for 30 min with 4 vol% H_2/He. The feed gases were controlled by mass flow controllers (Bronkhorst) and set to a total flow of $30\ ml\ min^{-1}$. All of the gases were 4 vol% in He, and the ratio used for the catalytic combustion of propylene was $C_3H_6/O_2 = 1/9$ (large excess of oxygen). The reaction was started after stabilization at room temperature for at least 30 min. The experiments were performed in a temperature-programmed way: the temperature was slowly increased or decreased ($5\ °C\ min^{-1}$) between room temperature and 400 °C. The temperature ramp of $5\ °C\ min^{-1}$ was considered to be sufficiently slow to reach a pseudo-steady state at every point. Each experiment consisted of at least two heating-cooling cycles, to monitor pos-

sible hysteresis and catalyst deactivation processes. The effluent stream of the propene oxidation reaction was analyzed every minute with either a gas chromatograph (Chrompack CP-9001) equipped with a Haysep N column, a methanizer, and FID detector, or a quadrupole mass spectrometer (Balzers Q422). Usually, the turnover frequency (TOF), defined as the catalytic activity per surface metal atom, is a realistic parameter for a comparison of the catalyst performance. In general, CO and H_2 titration is used to determine the number of exposed metal atoms. For gold-based catalysts, this titration method is not applicable because of the weak adsorption of these molecules on the Au surface. Therefore, to compare the catalytic performance of different catalysts tested in this study, the conversion achieved during the second heating cycle will be used.

3. Results and discussion

Table 1 summarizes the gold loading, the average size of gold particles for fresh and spent catalysts as determined by XRD measurements, and the total and metallic surface areas of the catalysts. The details are described below. The same table contains the results of the catalytic performance tests expressed in terms of $T_{95\%}$, which corresponds to the temperature needed to achieve 95% propene conversion during the second heating stage. In general the catalysts performed slightly better during the first heating-cooling cycle, but the difference between the cycles did not exceed 30–40 °C. Results obtained during the third or fourth heating cycle were similar to those obtained during the second run.

The results obtained for the gold loading show a relatively small variation from the intended results (5 wt%). The BET total surface area is above 200 $m^2\,g^{-1}$ for all samples. Gold deposition (Au/Al_2O_3 catalyst) did not result in a significant change in the total surface area (260 $m^2\,g^{-1}$ compared with 275 $m^2\,g^{-1}$ for the Al_2O_3 support). However, the total surface area was 207 $m^2\,g^{-1}$ for $Au/CoO_x/Al_2O_3$ and 218 $m^2\,g^{-1}$ for $Au/CeO_x/Al_2O_3$. The additive probably blocks some of the Al_2O_3 pores during the vacuum impregnation step, resulting in a decrease in S_{BET} up to a maximum of 25%. Freshly prepared catalysts and spent catalysts were subjected to XRD, and the results given in Table 1 show that the size of the gold particles is preserved during the reaction test. The only exception is $Au/MnO_x/Al_2O_3$: relatively large

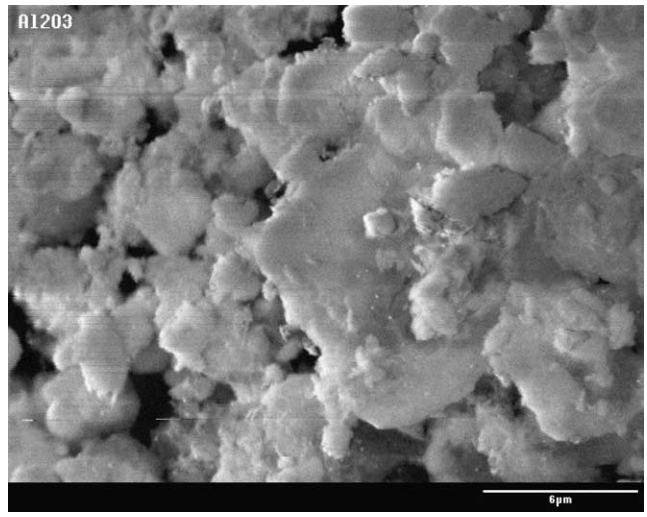

Fig. 1. Scanning electron microscopy (SEM) picture of Al_2O_3.

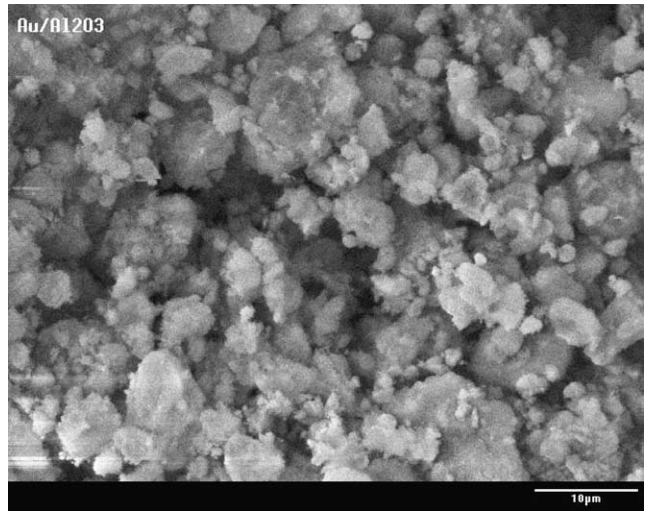

Fig. 2. Scanning electron microscopy (SEM) picture of Au/Al_2O_3.

Table 1
Catalysts characterization and catalytic performance in propene oxidation for Au/Al_2O_3, $Au/CeO_x/Al_2O_3$, $Au/CoO_x/Al_2O_3$, $Au/MnO_x/Al_2O_3$, and $Au/FeO_x/Al_2O_3$. C_3H_6:O_2 ratio is 1:9

Catalyst	Au (wt%)	S_{BET} ($m^2\,g^{-1}$)	$d_{Au}^{XRD,f}$ (nm)	$d_{Au}^{XRD,s}$ (nm)	d_{Au}^{HRTEM} (nm)	S_{Au}^{XRD} $m^2\,g^{-1}$	$T_{95\%}$ (°C)	X_{Max} (%)
$Au/CeO_x/Al_2O_3$	4.5	218	< 3.0	< 3.0	1.7 ± 0.2	–	224	20
$Au/CoO_x/Al_2O_3$	4.3	207	5.0 ± 0.1	5.9 ± 0.1	–	2.2	319	n.m.
$Au/MnO_x/Al_2O_3$	4.3	222	8.0 ± 0.1	11.0 ± 0.1	4.9 ± 0.3	1.4	294	10
$Au/FeO_x/Al_2O_3$	4.4	234	< 3.0	3.1 ± 0.2	–	–	273	n.m.
CeO_x/Al_2O_3	–	–	–	–	–	–	> 400	26
Au/Al_2O_3	4.1	260	4.3 ± 0.1	4.5 ± 0.2	5.2 ± 0.3	2.4	417	0
Al_2O_3	–	275	–	–	–	–	> 400	–

Mean diameters of gold particles, as determined by X-ray diffraction measurements: $d_{Au}^{XRD,f}$, fresh catalysts; $d_{Au}^{XRD,s}$, spent catalysts; and determined by HRTEM measurements: d_{Au}^{HRTEM}, fresh catalysts. X_{Max}, maximum propene conversion in the absence of O_2 in the gas stream. n.m.: not measured.

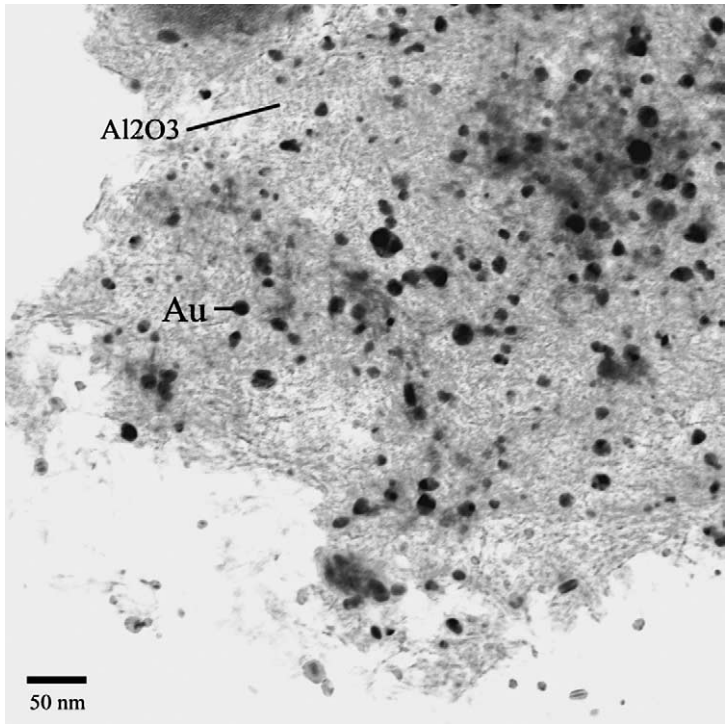

Fig. 3. HRTEM micrograph of Au/Al_2O_3. Gold particles are visible as black dots on the support.

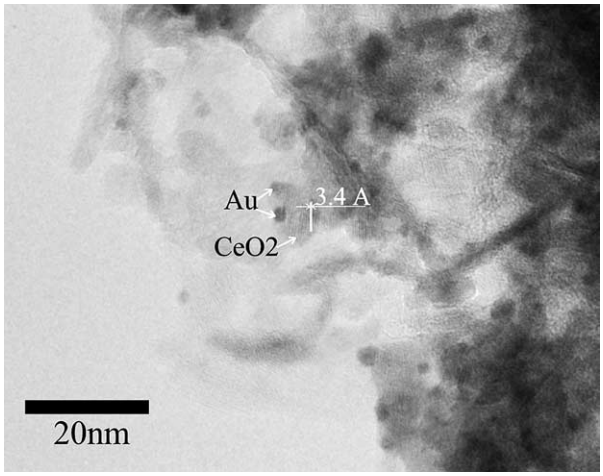

Fig. 4. HRTEM micrograph of $Au/CeO_x/Al_2O_3$ (black dots represent Au particles, dark gray dots-ceria and light gray regions-alumina).

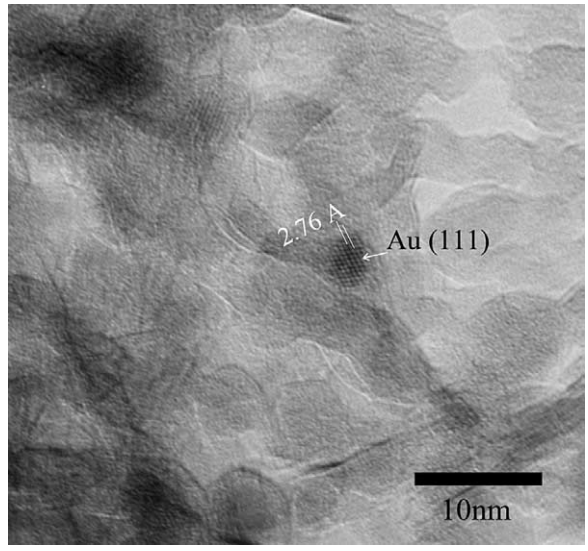

Fig. 5. HRTEM micrograph of $Au/CeO_x/Al_2O_3$. The lattice spacing of Au was found to be 2.76 Å.

particles were found for the as-prepared sample; XRD revealed an average of gold particles around 8.1 nm. The spent $Au/MnO_x/Al_2O_3$ shows an average around 11 nm. However, the catalytic activity of $Au/MnO_x/Al_2O_3$ is very high (see Table 1). This result suggests that for this type of catalyst, which contains an "active" oxide as MnO_x, the mean diameter of particles might be not very crucial for obtaining an active catalyst. However, we cannot rule out the possibility that $Au/MnO_x/Al_2O_3$ also contains very small gold crystallites below the XRD detection limit (~ 3 nm). A similar effect is found for $Au/CoO_x/Al_2O_3$, which exhibits a good performance in propene oxidation and whose average gold particles are around 5 nm for the fresh sample. In addition, no diffraction lines for Au_2O_3 or Au_2O were found for any catalysts.

Based on the XRD measurements, the gold surface area of the catalysts has been estimated; the results are also summarized in Table 1. The calculations have been made assuming that the gold particles are hemispherical in shape, with the flat side on the support. The results may be considered a relative measure of the available gold surface area. Based on XRD results, it is found that the Au sur-

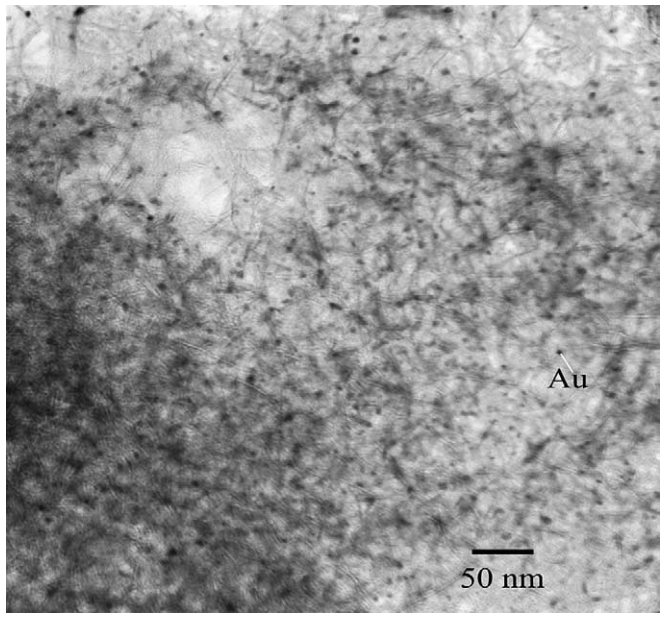

Fig. 6. HRTEM micrograph of $Au/MnO_x/Al_2O_3$.

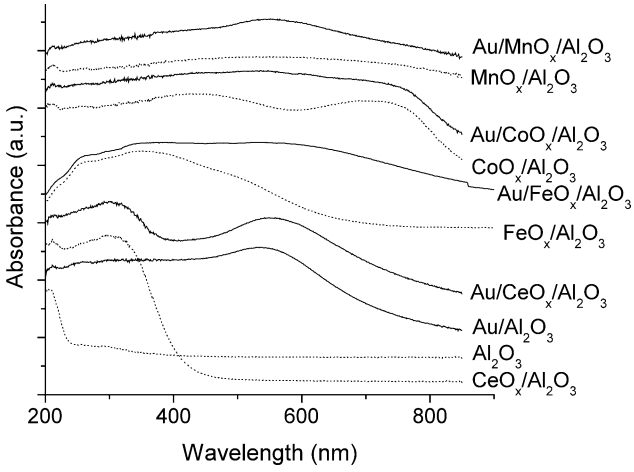

Fig. 7. DR/UV–Vis optical spectra of different gold-based catalysts.

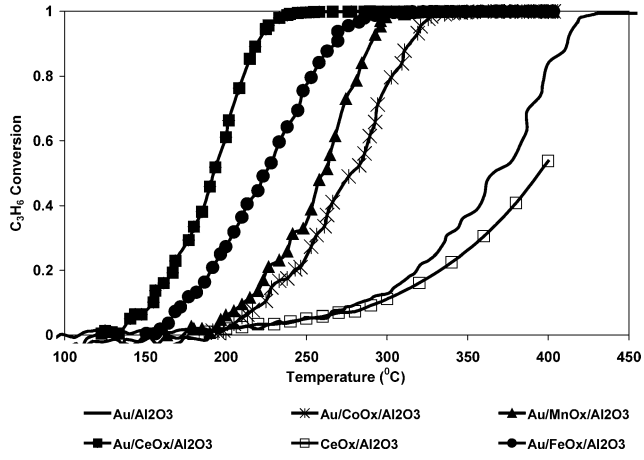

Fig. 8. Catalytic activity performance of Au/Al_2O_3, $Au/CeO_x/Al_2O_3$, $Au/CoO_x/Al_2O_3$, $Au/MnO_x/Al_2O_3$, $Au/FeO_x/Al_2O_3$, and CeO_x/Al_2O_3. Reactant ratio: $C_3H_6{:}O_2 = 1{:}9$, total flow rate: 30 ml min^{-1}.

face area varies between 1.4 $m^2\,g^{-1}$ ($Au/MnO_x/Al_2O_3$) and 2.4 $m^2\,g^{-1}$ (Au/Al_2O_3). However, a complete ranking of the catalysts based on the variation of the Au surface area cannot be made, since XRD was unable to detect any Au signal for $Au/CeO_x/Al_2O_3$ and $Au/FeO_x/Al_2O_3$. Additional HRTEM measurements are necessary. For some of the oxides it was possible to identify their formal oxidation state, but not for all. Because of their relatively low loading, these oxides are presumably highly dispersed over alumina, which makes the interpretation of the XRD spectra difficult.

Scanning electron microscopy (SEM) was performed to visualize possible macroscopic changes in the alumina structure after gold deposition. The two pictures presented in Figs. 1 and 2, of Al_2O_3 and Au/Al_2O_3, respectively, demonstrate that the support is preserved after Au deposition.

Fig. 3 shows a typical HRTEM image of the gold particles for Au/Al_2O_3. The gold particles (black dots in Fig. 3) are fairly homogeneously distributed over the support and have an average diameter of 5.2 nm. Two HRTEM micrographs of $Au/CeO_x/Al_2O_3$ catalyst are presented in Figs. 4 and 5. It is noteworthy that metallic gold particles (black dots in Fig. 4) are mainly located on the crystalline ceria (dark gray dots) and to a lesser extent on alumina (light gray regions). Fig. 5 shows the lattice spacing of Au, 2.76 Å, which corresponds to the Au(111) reflection. The mean diameter of the gold particles, as determined by counting at least 200 particles, was found to be around 1.7 nm.

Fig. 6 shows the HRTEM micrograph of $Au/MnO_x/Al_2O_3$. The gold particles are visible as black dots and are rather homogeneously distributed over the support, but are larger than in the case of $Au/CeO_x/Al_2O_3$, $d_{Au} = 4.9$ nm.

The metallic gold surface area of $Au/CeO_x/Al_2O_3$ as determined by HRTEM measurements is 7.1 $m^2\,g^{-1}$. For

$Au/MnO_x/Al_2O_3$ catalyst it is 2.4 $m^2\ g^{-1}$, and for Au/Al_2O_3, 1.5 $m^2\ g^{-1}$. The corresponding Au dispersion was estimated to be around 52% for $Au/CeO_x/Al_2O_3$, which is much higher than the Au dispersion of $Au/MnO_x/Al_2O_3$, 20%, and that of Au/Al_2O_3, 11.5%. A large dispersion/metallic surface area would imply a highly active catalyst. Hence, $Au/CeO_x/Al_2O_3$ would perform the best from the series if the noble metal were the only active phase.

The optical spectra of $Au/MO_x/Al_2O_3$ are presented in Fig. 7. For comparison, the same figure also depicts the spectra of the corresponding supports. The typical plasmon resonance peak of metallic gold around 550 nm is a general characteristic for all samples. Other additional absorption bands (due to ionic gold or partly charged Au nanoclusters) have not been detected in the optical spectra (absorption bands below 500 nm). In principle, a direct correlation should exist between the mean particle diameter as determined by XRD and/or HRTEM and the peak and shape position in DR/UV–Vis spectra. A sharper peak in DR/UV–Vis implies larger Au particles. However, other factors may also influence the optical spectra, such as the surrounding environment and the interaction between gold and support [17].

The catalytic performance expressed in terms of the temperature needed to reach 95% propene conversion is summarized in Table 1. The catalytic performance of the samples over the whole temperature range is illustrated in Fig. 8. In addition, the catalytic performance of CeO_x/Al_2O_3 is also depicted, for comparison. The most active catalyst is $Au/CeO_x/Al_2O_3$, with a $T_{95\%} = 224\,^{\circ}C$. This catalyst also shows a good stability during the catalytic runs (compare $d_{Au}^{XRD,f}$ with $d_{Au}^{XRD,s}$ in Table 1). The next catalyst able to almost fully convert C_3H_6 into CO_2 at a temperature as low as 294 °C is $Au/FeO_x/Al_2O_3$, followed by $Au/MnO_x/Al_2O_3$ and $Au/CoO_x/Al_2O_3$.

The supports were also tested for C_3H_6 oxidation, and no noticeable conversion was found, with the exception of CeO_x/Al_2O_3 (see Fig. 8). It is interesting to note that $Au/MnO_x/Al_2O_3$, with relatively big Au particles (8 nm), is an active catalyst and converts C_3H_6 at a temperature lower than, for instance, $Au/CoO_x/Al_2O_3$. Based on the above-presented results, $Au/CeO_x/Al_2O_3$ can be considered the most promising catalyst of the series, not only because it converts C_3H_6 into CO_2 at the lowest temperature, but also because it shows a high stability. Its performance was stable even after 8 h on stream. In fact, all gold-based catalysts used in this study display a good stability. The catalytic performance was stable during the 8-h test, and the d_{Au}^{XRD} did not increase very much (see Table 1). $Au/CeO_x/Al_2O_3$ appears to be the best candidate for practical applications because of its lowest light off temperature, small gold particles, and high Au dispersion.

It appears that for catalysts containing a transition metal oxide as additive, the mean diameter of the gold particles (as determined by XRD and/or HRTEM) is not very crucial for obtaining an active catalyst. The reason for this may reside in the intrinsic properties of the additives, which may act not only as a structural promoter (by stabilizing gold particles against sintering, a phenomenon which starts early in the preparation step), but also as a chemical promoter, or as a co-catalyst. It has already been mentioned that the mixed oxides CeO_x/Al_2O_3, MnO_x/Al_2O_3, CoO_x/Al_2O_3, and FeO_x/Al_2O_3 are not very active in C_3H_6 oxidation under the reaction conditions used in this study. Thus, the question is: how do these oxides interact with gold and/or participate in the catalytic process?

Ceria is very well known for its oxygen storage capacity (OSC), defined as the capacity to release/accept oxygen under fuel-rich/lean conditions in the gas stream. Centeno and co-workers [34] have studied the catalytic combustion of VOCs on $Au/CeO_x/Al_2O_3$, and they concluded that the presence of cerium ions exerts a positive influence on the fixation and the final dispersion of gold on alumina support. In addition, ceria stabilizes the gold particles with low crystallite size. In addition to these beneficial features, ceria, because of its redox properties, may improve the catalytic behavior of the catalyst by increasing the supply of active oxygen. Similar conclusions were proposed by Scire et al. [21] in their study of VOC oxidation over Au/CeO_2. The mechanism of hydrocarbon oxidation over ceria and other reducible metal oxides is usually considered to be of the redox or Mars and van Krevelen type [9,10,21,34]. The key steps of this mechanism are believed to be the supply of active oxygen by the readily reducible oxide and its reoxidation by oxygen. In addition, Fu et al. [35] discussed the catalytic performance of $Au\text{-}CeO_2$ for the WGS reaction in terms of the mean diameter of CeO_2 particles. Apparently, the interfacial effect created by metal-support interaction is more important than the mean diameter of gold particles. Moreover, because the active oxygen is supplied by CeO_2, the dimensions of the ceria particles are important. In the present study the mean diameter of CeO_2, as estimated from the FWHM of the main peak from $2\theta = 28.54\,^{\circ}$ (XRD), was found to be around 9 nm. This value is relatively close to those reported by Fu et al. [35]. Moreover, according to X-ray diffraction measurements, no significant change in the diameter of ceria particles was detected for the spent catalyst, implying that ceria is stable during the catalytic test.

The oxygen availability of CeO_x and, in turn, the presence of a Mars and van Krevelen mechanism in propene oxidation were examined over pre-reduced (H_2, 300 °C, 30 min) CeO_x/Al_2O_3. During the catalytic run, oxygen was replaced with argon. Hence, the feed passing through the catalyst bed consisted of 4% C_3H_6 in He and Ar. Interestingly, in addition to propene consumption and water formation, a relatively large amount of CO_2 was detected. This is a direct indication that, although CeO_x/Al_2O_3 has already been subjected to mild hydrogen pretreatment at 300 °C for 30 min prior to the reaction, there is still lattice oxygen available for reaction with C_3H_6 to form CO_2 and H_2O. The propene consumption and the water and carbon dioxide production are depicted in Fig. 9. Clearly, CO_2 is formed and C_3H_6 is consumed around 350 °C, the same temperature range at which

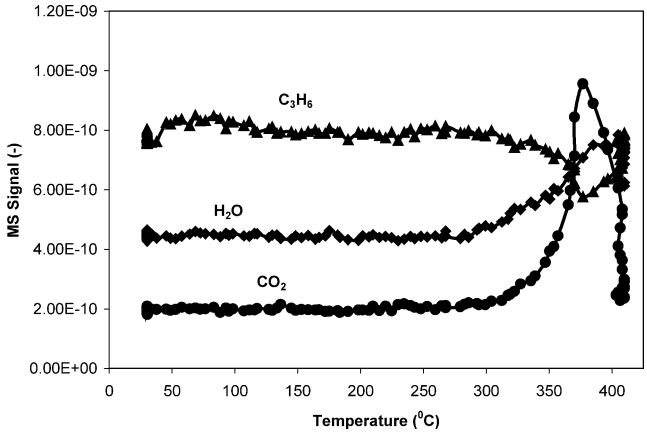

Fig. 9. The change in the signal of C_3H_6, H_2O, and CO_2 when a feed of 4% C_3H_6/He has been passed over CeO_x/Al_2O_3 catalyst bed.

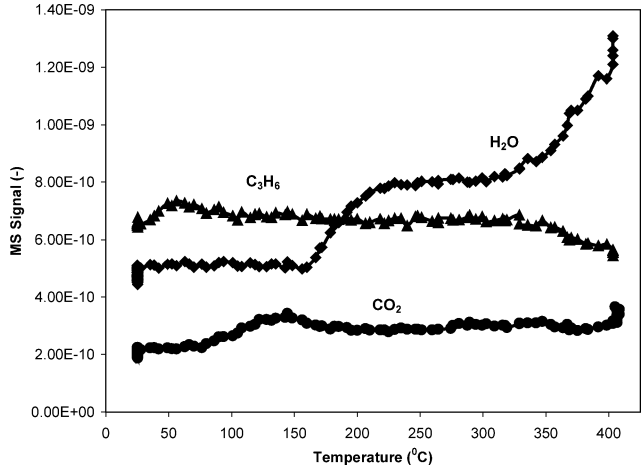

Fig. 10. The change in the signal of C_3H_6, H_2O, and CO_2 when a feed of 4% C_3H_6/He has been passed over $Au/CeO_x/Al_2O_3$ catalyst bed.

C_3H_6 is oxidized in the presence of O_2 (see Fig. 8). It also has to be mentioned that at the end of the experiment, some coke deposition was visible on the topmost part of the catalyst bed. Apparently, the rate of C deposition was higher than its transformation into CO_2. It appears that in the case of CeO_x/Al_2O_3, the Mars and van Krevelen mechanism is valid, inasmuch as the lattice oxygen of CeO_2 is accessible for the reaction with C_3H_6.

A similar experiment was performed over a mildly pre-reduced $Au/CeO_x/Al_2O_3$ catalyst. As should be expected, CO_2 and H_2O are formed and propene is consumed in the same temperature range ($\sim 350\,^{\circ}C$) as found for CeO_x/Al_2O_3. The C_3H_6 conversion is lower than was found for CeO_x/Al_2O_3. Nevertheless, a 20% conversion of C_3H_6 could be achieved over $Au/CeO_x/Al_2O_3$ in this temperature range without O_2 in the feed (see Table 1, last column). The C_3H_6 consumption and the water and carbon dioxide production obtained during this catalytic run over gold containing CeO_x/Al_2O_3 are shown in Fig. 10. Interestingly, CO_2 and H_2O are also formed in the temperature range at which propene is oxidized by O_2 over $Au/CeO_x/Al_2O_3$, that is, around 150 °C. Thus, by this experiment it is proved that the oxygen of ceria is highly mobile and plays an active role in C_3H_6 oxidation into CO_2. X-ray diffraction experiments performed on the spent $Au/CeO_x/Al_2O_3$ did not reveal any change in the structure of CeO_2 or in that of Au. Probably only the near-surface oxygen, known as a highly mobile species, had an active role in the oxidation, and the temperature and reaction conditions attained were not sufficient to convert the CeO_2 to Ce_2O_3. In addition, no detectable change in the structure of Au was detected by XRD, and the average size of the gold particles as estimated by the FWHM of $2\theta = 38.2\,^{\circ}$ was not affected by this experiment. Coke deposition has not been observed for $Au/CeO_x/Al_2O_3$. Apparently the presence of gold prevents coke formation during C_3H_6 oxidation.

To examine any direct participation of MnO_x in propene oxidation, an experiment similar to the one described for $Au/CeO_x/Al_2O_3$ was performed with mildly pre-reduced $Au/MnO_x/Al_2O_3$. In the absence of O_2, a maximum C_3H_6 conversion of 10% was found in the first heating run (see Table 1). In addition, XRD measurements performed on the spent $Au/MnO_x/Al_2O_3$ revealed a dramatic change in the structure of the catalyst. Fig. 11 shows the XRD patterns for MnO_x/Al_2O_3, fresh $Au/MnO_x/Al_2O_3$, and spent $Au/MnO_x/Al_2O_3$. One can see that the XRD pattern of fresh $Au/MnO_x/Al_2O_3$ consists of several peaks that belong either to MnO_x/Al_2O_3 ($2\theta = 37.2°$, $2\theta = 43.3°$), or to metallic gold ($2\theta = 38.2°$, $2\theta = 44.3°$). JCPDS powder diffraction database files [36] have confirmed that manganese is in the form of MnO_2 in both the support and the fresh gold-based catalyst. The situation is changed for spent $Au/MnO_x/Al_2O_3$ (see Fig. 11). First of all, the XRD pattern of MnO_2 had disappeared, and new peaks at $2\theta = 34.8°$ and $2\theta = 40.5°$ appeared. According to [36], these peaks comprise the fingerprint of MnO. In addition, the peak intensity of metallic gold increases, especially that for $2\theta = 44.3°$. Thus, $Au/MnO_x/Al_2O_3$ suffers drastic, irreversible changes upon reaction with propene in the absence of O_2, whereas with $Au/CeO_x/Al_2O_3$ the whole structure of ceria is preserved in the form of CeO_2 and only a minor reduction takes place. From thermodynamic data, the enthalpy of formation of MnO by the reduction of MnO_2 is 135 kJ mol^{-1}. On the other hand, the formation enthalpy of Ce_2O_3 as a result of CeO_2 reduction is much higher, 378 kJ mol^{-1}. These data confirm our experimental results, that the reduction of MnO_2 to MnO proceeds more easily than the reduction of CeO_2 to Ce_2O_3. As a consequence, MnO is obtained with only C_3H_6 in the gas stream, whereas CeO_2 is little affected by the reducing gas.

On the basis of these results our conclusion is that, indeed, the Mars–van Krevelen mechanism plays a significant role in propene oxidation over $Au/CeO_x/Al_2O_3$ and $Au/TMO/Al_2O_3$ (TMO, transition metal oxide) catalysts. Hence, the readily reducible oxide can provide the active oxygen for the reaction to take place, and, probably, there is a direct relationship between oxygen availability (based

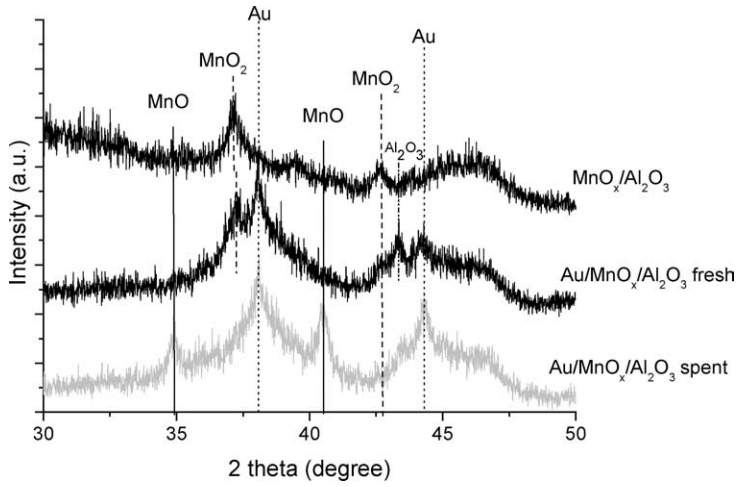

Fig. 11. XRD patters of MnO_x/Al_2O_3, fresh-$Au/MnO_x/Al_2O_3$ and spent-$Au/MnO_x/Al_2O_3$.

on our calculations, mainly the near-surface oxygen of ceria is involved in the reaction) and the catalytic performance. This oxidation mechanism may also explain the gold particle size effect, that is, why $Au/MnO_x/Al_2O_3$ ($d_{Au}^{XRD} = 8$ nm) is a very effective catalyst in C_3H_6 oxidation, in spite of its large gold particles: the active oxygen is provided by MnO_x, and propene may be activated on Au or at the interface gold/support.

Other factors may also play a role in the observed catalytic performance of $Au/MO_x/Al_2O_3$. Density-functional calculations for Au clusters show that O_2 and CO can adsorb Au atoms if the coordination number (CN) is less than 8 [37]. In turn, the concentration of low coordinated Au atoms depends on both the size and the shape of the particle [38]. In our case we did not find a direct relationship between the size of gold particles and the catalytic activity in C_3H_6 oxidation (see above), but information on the shape of the particles is not available. On the other hand, the interaction of Au with the support is stronger on a surface with oxygen defects, an increased number of steps, or adatoms. As already discussed, ceria, for example, may have a relatively high concentration of oxygen vacancies because of its very facile redox cycle Ce^{4+}/Ce^{3+}. As a result, the characteristics of the support may influence both the Au anchoring process and the overall catalytic activity.

In conclusion, gold-based catalysts that contain a transition metal oxide or ceria are highly active in propene oxidation. The role of the oxide is twofold: it stabilizes the gold particles against sintering (ceria) and provides active oxygen for the reaction (CeO_x, MnO_x, CoO_x, or FeO_x) via the Mars and van Krevelen mechanism.

4. Conclusions

This paper describes the characterization and the catalytic performance in C_3H_6 oxidation of various gold-based catalysts. In general, the preparation method and the pretreatment used result in nanosized gold particles in the metallic state that are highly active in propene oxidation. The catalytic activity of Au/Al_2O_3 is improved by the addition of transition metal oxides (TMOs) and ceria. These additives can act as a structural promoter and/or as a cocatalyst. The most active catalyst contains ceria. The gold particles are stabilized against sintering in the presence of ceria. In addition, it was proved experimentally that the lattice oxygen of the oxide plays an active role in C_3H_6 oxidation via the Mars and van Krevelen mechanism.

Acknowledgments

A.C. Gluhoi would like to express her gratitude to Dr. P. Marginean and Dr. M. Avalos Borja for fruitful discussions and to I. Gradilla Martínez, F. Ruiz Medina, and E. Flores for technical support. The Netherlands Organization for Scientific Research (NWO) (Grant NWO/CW 99037 and NWO #047.015.003), and grants from CONACYT (42568-Q) and PAPIIT-UNAM (IN109003) (Mexico) are gratefully acknowledged for financial support.

References

[1] D.L. Trimm, Appl. Cat. 7 (1983) 249.
[2] J.E. Germain, Catalytic Conversion of Hydrocarbons, Academic Press, 1967.
[3] G.K. Boreskov, Catalysis Science and Technology, vol. 3, Springer, Berlin, 1985.
[4] E. Garbowski, M. Guenin, M.C. Marion, M. Primet, Appl. Catal. 64 (1990) 209.
[5] L.Y. Margolis, Adv. Catal. 14 (1963) 429.
[6] A. Terleckibaricevic, B. Grbic, D. Jovanovic, S. Angelov, D. Mehandziev, C. Marinova, P. Kirilovstefanov, Appl. Catal. 47 (1989) 145.
[7] K. Tabata, M. Misono, Catal. Today 8 (1990) 249.
[8] T. Seiyama, Catal. Rev. Sci. Eng. 34 (1992) 281.
[9] E. Finocchio, G. Busca, V. Lerenzelli, V.S. Escribano, J. Chem. Soc.-Farad. Trans. 92 (1996) 1587.

[10] E. Finocchio, R.J. Willey, G. Busca, V. Lorenzelli, J. Chem. Soc.-Farad. Trans. 93 (1997) 175.
[11] M. Haruta, N. Yamada, T. Kobayashi, S. Iijima, J. Catal. 115 (1989) 301.
[12] S.D. Gardner, G.B. Hoflund, B.T. Upchurch, D.R. Schryer, E.J. Kielin, J. Schryer, J. Catal. 129 (1991) 114.
[13] S.D. Lin, M. Bollinger, M.A. Vannice, Catal. Lett. 17 (1993) 245.
[14] A. Ueda, T. Oshima, M. Haruta, Appl. Catal. B 12 (1997) 81.
[15] M.A.P. Dekkers, M.J. Lippits, B.E. Nieuwenhuys, Catal. Today 54 (1999) 381.
[16] A.C. Gluhoi, M.A.P. Dekkers, B.E. Nieuwenhuys, J. Catal. 219 (2003) 197.
[17] P. Claus, A. Bruckner, C. Mohr, H. Hofmeister, J. Am. Chem. Soc. 122 (2000) 11430.
[18] D. Andreeva, V. Idakiev, T. Tabakova, A. Andreev, J. Catal. 158 (1996) 354.
[19] S.D. Lin, A.C. Gluhoi, B.E. Nieuwenhuys, Catal. Today 90 (2004) 3.
[20] S. Minico, S. Scire, C. Crisafulli, R. Maggiore, S. Galvagno, Appl. Catal. B 28 (2000) 245.
[21] S. Scire, S. Minico, C. Crisafulli, C. Satriano, A. Pistone, Appl. Catal. B 40 (2003) 43.
[22] N.A. Hodge, C.J. Kiely, R. Whyman, M.R.H. Siddiqui, G.J. Hutchings, Q.A. Pankhurst, F.E. Wagner, R.R. Rajaram, S.E. Golunski, Catal. Today 72 (2002) 133.
[23] S.-O. Oh, C.K. Costello, C. Cheung, H.H. Kung, M.C. Kung, Stud. Surf. Sci. Catal. 139 (2001) 375.
[24] M. Haruta, M. Date, Appl. Catal. A 222 (2001) 427.
[25] J. Guzman, B.C. Gates, J. Phys. Chem. B 106 (2002) 7659.
[26] M. Haruta, T. Kobayashi, N. Yamada, Chem. Lett. 2 (1987) 405.
[27] M. Haruta, S. Tsubota, T. Kobayashi, H. Kageyama, M.J. Genet, B. Delmon, J. Catal. 144 (1993) 175.
[28] G.B. Hoflund, S.D. Gardner, D.R. Schryer, B.T. Upchurch, E.J. Kielin, Langmuir 11 (1995) 3431.
[29] M. Bollinger, M.A. Vannice, Appl. Catal. B 8 (1996) 417.
[30] E.P.J. Mallens, J.H.B.J. Hoebink, G.B. Marin, J. Catal. 160 (1996) 222.
[31] G.R. Bamwenda, A. Obuchi, A. Ogata, J. Oi, S. Kushiyama, K. Mizuno, J. Mol. Catal. A 126 (1997) 151.
[32] C.C. Chien, W.P. Chuang, T.J. Huang, Appl. Catal. A 131 (1995) 73.
[33] H.H. Kung, Stud. Surf. Sci. Catal. 45 (1989) 86.
[34] M.A. Centeno, M. Paulis, M. Montes, J.A. Odriozola, Appl. Catal. A 234 (2002) 65.
[35] Q. Fu, A. Weber, M. Flytzani-Stephanopoulos, Catal. Lett. 77 (2001) 87.
[36] JCPDS Powder Diffraction File, International Centre for Diffraction Data.
[37] N. Lopez, J.K. Norskov, J. Am. Chem. Soc. 124 (2002) 11262.
[38] N. Lopez, J.K. Norskov, T.V.W. Janssens, A. Carlsson, A. Puig-Molina, B.S. Clausen, J.D. Grunwaldt, J. Catal. 225 (2004) 86.